論文 / 著書情報
Article / Book Information

Title	Strain ageing effects in reinforcing bars subjected to earthquake damage
Authors	Koshin OKAMURA, Alex SHEGAY, Daiki SATO, Masaki MAEDA
Citation	20th Proceedings of the fib Symposium 2024, pp. 2471-2480
Pub. date	2024, 11
Note	Reproduced from the 20th fib Symposium Proceedings – ReConStruct - Resilient Concrete Structures, held in Christchurch from 11-13 November 2024, paper "Strain ageing effects in reinforcing bars subjected to earthquake damage ” , authors "Koshin OKAMURA, Alex SHEGAY, Daiki SATO, Masaki MAEDA" - pages 2471-2480 - from the International Federation for Structural Concrete (fib).

Strain ageing effects in reinforcing bars subjected to earthquake damage

Koshin OKAMURA[1[]] and Alex SHEGAY[2[]], Daiki SATO[1[]], Masaki MAEDA[3[].]

[1] Tokyo Institute of Technology
[2] University of Auckland
[3] Tohoku University

Abstract. One of the factors affecting repair feasibility of buildings damaged by earthquakes is the potential effects of strain ageing of reinforcement. Since strain ageing can lead to an increase in structural member strength and ductility reduction, the strength hierarchy set through capacity design disruptions can be disrupted leading unexpected seismic response of individual members or the structure as a whole. In this study, from simple tensile tests on reinforcing bars, we identified three factors that affect strain ageing: vanadium content, ageing period, and pre - strain, and constructed a formula for predicting changes in reinforcing bar properties using these factors. And, from seismic response analysis of Japanese RC buildings and experiments on RC beam members, the maximum strain of reinforcing bars was 1.7% and 2.3%, respectively, in response to design level 2 earthquake motion. Using the simple relationships between the expected strains of members in this analytical model, we created a building model that adjusted for the effects of strain ageing on reinforcing bars after an earthquake, and performed seismic response analysis again. As a result, no major differences were observed in future seismic responses. The reason for this is thought to be that Japanese RC buildings have high rigidity and yield is limited.
Keywords: Strain ageing, Repair, Steel reinforcement, Prediction model, Beam experiment

1 Introduction

In recent years, the increasing desire for sustainable and reusable buildings, the significance of repairing buildings damaged by earthquakes has been increasing. Strain ageing is one of the factors that changes the seismic performance of buildings after repair. As shown in Fig. 1, strain ageing is a phenomenon that occurs in steel over time after plastic strain is applied, which causes a decrease in ductility, increase in strength, and a reappearance of the yield point. Strain ageing of reinforcing bars can affect the seismic performance of reinforced concreted (RC) buildings, because a decrease in ductility of reinforcing bars can cause brittle failure of members, and a non-uniform increase in strength of all members can cause a change in the failure mode of buildings. An example of an unfavorable scenario that can be result by strain ageing is an increase in the yielding strength of beams over time following an initial earthquake, which would reduce the beam-column moment ratio and cause a transition of frame response from a beam-sway (beam yielding) to a column-sway (column yielding) collapse mechanism.

Although there have been some previous studies on strain ageing[2-5)], no predictive models have been developed, and no quantitative predictions of the effects have been made for RC buildings or steel reinforcement. Therefore, the objective of this paper consists in three parts. The first objective is to summarize the factors that affect the change in properties of reinforcing bars due to strain ageing from simple tension experiments, and to introduce a model to quantify these effects. The second objective is

to use this model to quantify the magnitude of strain ageing expected in reinforcing bars of typical Japanese RC buildings following earthquake events. Finally, the effect of strain aged reinforcing bars on the future seismic performance of RC buildings will be examined via numerical modelling.

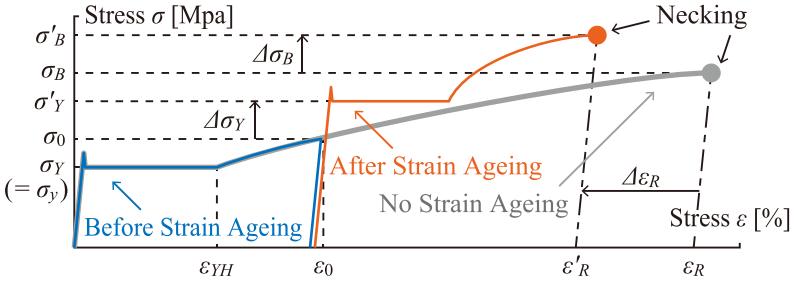

Fig. 1. Schematic diagram of stress-strain curve of reinforcing bars affected by strain ageing effects.

2 Overview of predictive model for strain ageing of reinforcing bars [1)]

2.1 Experiment outline

In this section, a predictive model of strain ageing effects previously developed by the authors[1)] will be introduced. The predictive model was developed from experimental data of reinforcing bars that were pulled to a specific strain (hereinafter referred to as 'pre-strain', ε_0), and after unloading were strain aged by allowing a specific amount of time to elapse (hereinafter referred to as 'ageing period', t_A). For bars with a long ageing period t_A (more than 3 months), strain ageing was accelerated by heat treatment procedures based on previous literature[2)]. Following the ageing period, the bars were tension tested to failure to measure differences in ductility and strength characteristics. In this paper, the strain at necking (i.e., the point at which the maximum tensile strength is reached and the strength starts to decrease) was used as an index for ductility, and ultimate tensile strength and yield strength were used as indices for strength. A total of 84 tensile tests were conducted.

2.2 Results on key contributing factors to strain ageing phenomenon

From the experimental results, it was determined that the general trend, regardless of the grade specification of the rebar, was as follows: (i) vanadium V content (λ_V) showed a clear inverse-linear relationship to the increase in yield strength due to strain ageing, (ii) the ageing period t_A was exponentially correlated to the increase in ultimate/yield strength and decrease in ductility, and (iii) the amount of pre-strain ε_0 was directly correlated to the *maximum* expected change in strength and ductility characteristics regardless of ageing period.

2.3 Prediction formula for strain ageing effects

The symbols used in the proposed prediction formula and the definition of property change are described first. As shown in the gray line in Fig. 1, the stress-strain curve of a normal rebar subjected to a tensile test first reaches its yield strength σ_Y, which is followed by a yield plateau and subsequent strain hardening at a strain value designated as ε_{YH}. After reaching ultimate strength capacity, σ_B, the rebar begins necking, gradually losing strength, and finally fracturing. The strain at the start of necking projected to the x-axis (using initial Young's modulus) is defined as the ε_R. If a virgin bar (shown by the blue line in Fig. 1), is unloaded and allowed to strain age part way through loading, the reloading stress σ - strain ε curve (shown as orange line in Fig.1) changes such that the yield plateau remerges, yield/ultimate strength increase and ductility decreases. The key quantities on the reloading $\sigma - \varepsilon$ curve are indicated with an apostrophe: with σ'_Y representing yield strength, σ'_B representing ultimate tensile strength, and ε'_R representing ductility.

The proposed predictive model utilizes dimensional metrics to quantify changes ductility β_R, ultimate tensile strength β_B, and yield strength β_Y. Definition for these metrics are provided in Eq. (1) ~ (3),

respectively. Conceptually, these metrics represent the ratio of the change in a given properties due to strain ageing as a percentage of the equivalent property had strain ageing not occurred.

$$\beta_R = \Delta\varepsilon_R/\varepsilon_R = (\varepsilon'_R - \varepsilon_R)/\varepsilon_R \quad (1)$$
$$\beta_B = \Delta\sigma_B/\sigma_B = (\sigma'_B - \sigma_B)/\sigma_B \quad (2)$$
$$\beta_Y = \Delta\sigma_Y/\sigma_Y = (\sigma'_Y - \sigma_0)/\sigma_y \quad (3)$$

The mathematical structure of the proposed model is shown in Eq. (4) ~ (6) and is based on the concept that each property change converges from a starting point of 0 to a maximum 'saturated' value with the passage of the ageing period t_A, and that the maximum value is a function of λ_V and ε_0. The maximum converged values are represented by f_R, f_B, and f_Y, as defined in Eq. (7) ~ (9).

$$\beta_R = -f_R(\lambda_V, \varepsilon_0)\left(1 - e^{-t_A/180}\right) \quad (4)$$
$$\beta_B = f_B(\lambda_V, \varepsilon_0)\left(1 - e^{-t_A/91}\right) \quad (5)$$
$$\beta_Y = f_Y(\lambda_V, \varepsilon_0)\left(1 - e^{-t_A/77}\right) \quad (6)$$
$$f_R(\lambda_V, \varepsilon_0) = 5.4(0.25 - 280\lambda_V)(-0.015 + 7.5\varepsilon_0) \geq 0 \quad (7)$$
$$f_B(\lambda_V, \varepsilon_0) = 29(0.064 - 210\lambda_V)(-0.0025 + 1.2\varepsilon_0) \geq 0 \quad (8)$$
$$f_Y(\lambda_V, \varepsilon_0) = (0.22 - 350\lambda_V)\varepsilon'_0 \geq 0$$
$$\varepsilon'_0 = \begin{cases} \varepsilon_0 > \varepsilon_{YH} : 1 \\ \varepsilon_0 \leq \varepsilon_{YH} : 1/4 \end{cases} \quad (9)$$

2.4 Verification of accuracy of prediction formula

The accuracy of the prediction equations is verified against the results of the experiments reported in this paper and those of previous studies. Eq. (10) ~ (12) show the equations for the predicted ductility ε'_R, ultimate tensile strength σ'_B, and yield strength σ'_Y after being affected by strain ageing.

$$\varepsilon'_R = \varepsilon_R \times (1 + \beta_R) \quad (10)$$
$$\sigma'_B = \sigma_B \times (1 + \beta_B) \quad (11)$$
$$\sigma'_Y = \sigma_0 + \sigma_Y \times \beta_Y \quad (12)$$

The relationship between the predictions and experimental measurements is shown in Fig. 2. Note that the experimental results reported in Momtahan et al.[4] and Pussegoda[5] did not have sufficient detail to calculate ε'_R, so these experimental results are not included in Fig. 2 (a). Fig. 2 (a) shows that the prediction equation for ductility loss generally agrees with the measured values, but the prediction error exceeds 10%. This is likely to the inaccuracy of the manual 'punch mark' method used to measure this quantity. On the other hand, Fig. 2 (b) and (c) show that the predicted and measured values for the increase in strength characteristics are generally within 10%. These models are applied to augment the performance of RC members in a building analyzed later in the paper.

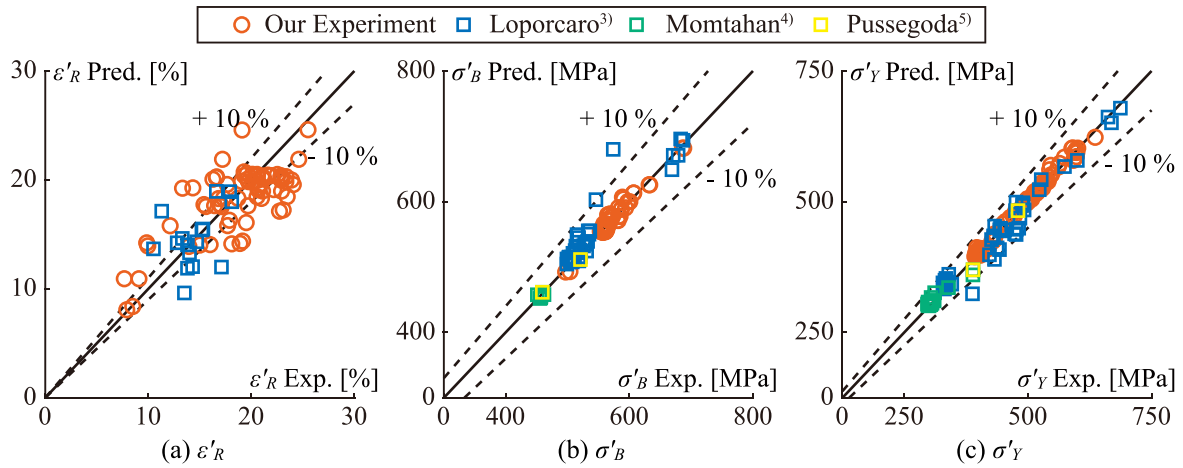

Fig. 2. Relationship between measured values and predicted values.

3 Strain of reinforcing bars during earthquake response

In the previous section, a prediction equation for the change in the properties of reinforcing bars due to strain ageing was introduced. In this section, the expected rebar strains in buildings subjected to earthquakes is estimated using analytical and experimental results. The expected rebar strains are then substituted into the model introduced in the previous section to predict the long-term change in rebar properties expected after the earthquake. In this paper, we will solely focus on the effects of change in yield strength β_Y as a rebar is typically not expected to reach ultimate tensile strain (unless buckling effects are considered).

3.1 Analytical investigation: earthquake response analysis overview

The building chosen for consideration is a 10-story RC building taken from the Book of Example Structural Design and Member Sections for Japan[6]. A lumped-plasticity frame model of this building is created using software RESP-D[7]. The plan and elevation drawings for this building are shown in Fig. 3. This building is a pure moment frame structure, and the structural design was carried out using allowable stress design principles. In addition, since the fracture of reinforcing bars is not assumed in this building model.

The building is analyzed in the X-direction using four seismic input waves of El Centro NS, Hachinohe EW, Hachinohe NS, and Taft EW. The ground motions are scaled such that the magnitude at which the peak ground velocity is 25 m/s is defined as the base case (this is consistent with what is often used as the Design Level 1 earthquake in Japan and is the demand level used to check against the damage avoidance limit state for structures, defined as a limiting inter-story drift of 0.5%). The building is analyzed for both 1.0 times and 2.0 times (the latter consistent with Design Level 2 earthquake in Japan, and is the demand level used to check that individual members have sufficient plastic rotation capacity) the input motion. Fig. 4 shows the acceleration response spectra S_A (5% damping) of the Design Level 1 demand (input motion spectra scaled by 1.0) and Design Level 2 demand (input motion spectra scaled by 2.0).

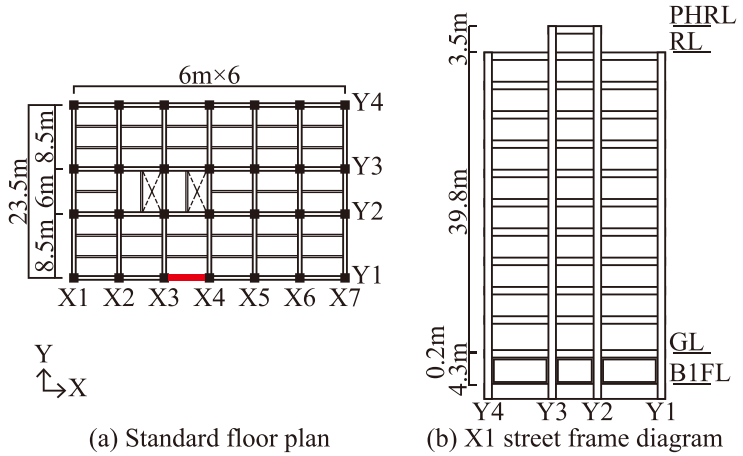

Fig. 3. Plan and elevation drawings of the study RC building.

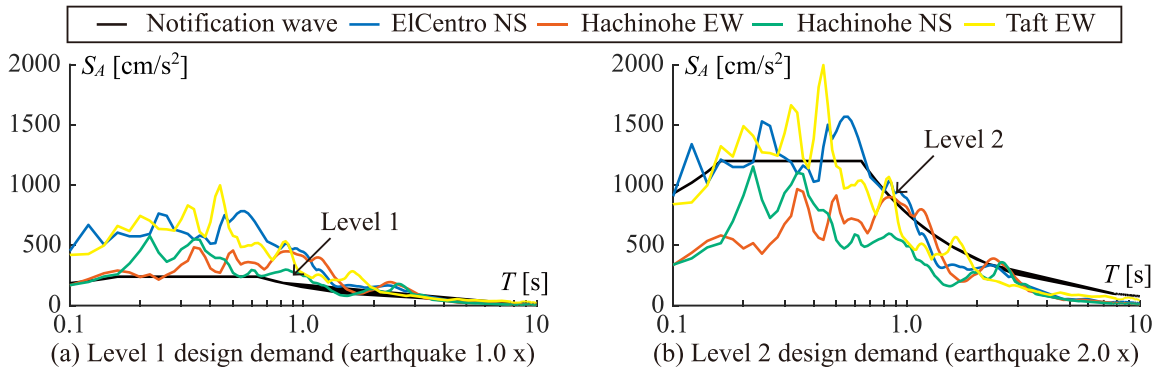

Fig. 4. Response acceleration spectra (5% damping).

3.2 Earthquake response analysis results

The analysis results show that the response of beams Y1@X3~4, shown in red in Fig. 3, was the largest on each floor. Table 2 shows the reinforcement characteristics of Y1@X3~4 beam. The analysis will focus on this beam location in the following sections.

For the floor with the largest response to each seismic wave, the moment-rotation ($M - \theta$) history of the response for each seismic wave, is shown in Fig. 5. Fig. 5 shows that the beam reaches the cracking moment for all seismic waves scaled to 1.0, and all but the Hachinohe NS waves scaled to 2.0 times resulted in beams yielding. The maximum rotation angle of the beam was 0.012 rad.

Table 2. Beam specifications of analysis model.

Floor	Dimension	Main reinforcement	Stirrups	Side bar
RF	400×850	6-D25	2-D13@200	2-D13
9~10F	500×900	10-D29	4-D13@200	4-D13
7~8F	550×950	12-D29	4-S13@200	4-D13
5~6F	550×950	12-D32	4-S13@150	4-D13
2~4F	550×1000	14-D32	4-S13@150	4-D13
1F	500×1000	10-D25	3-D13@200	4-D13

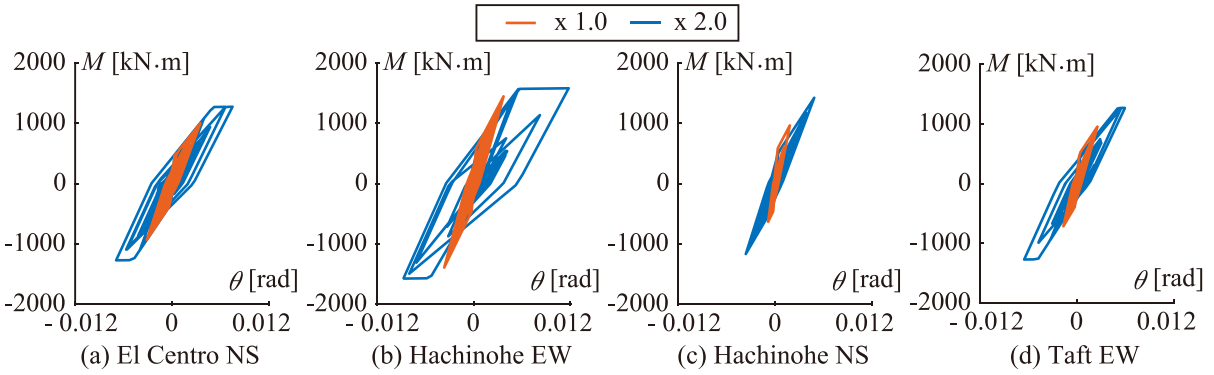

Fig. 5. Moment M - rotation angle θ relationship.

The strain time history of the beam's longitudinal bars is then derived from the time history of the beam's hinge rotation. The following assumptions were used in the derivation:

1) The hinge length L_P of the beam at flexural yield is half of the beam depth D and that all rotation is concentrated over this hinge length (mean strain assumption). The curvature φ in the hinge of the large beam is obtained as in equation (13) below.
2) Assuming that the plane-section assumption holds, the longitudinal strain ε in a given bar is obtained as the distance from the neutral axis to the bar multiplied by the curvature φ, as in equation (14)[8].

$$\varphi = \theta / L_p = 2\theta / D \tag{13}$$

$$\varepsilon_{avg} = \begin{cases} \varphi \cdot (d - x_n) (\text{Tension}) \\ \varphi \cdot (x_n - d') \ (\text{Compression}) \end{cases} \tag{14}$$

The relationship of ε_{avg} with respect to θ obtained in this derivation can be described via a single value, hereinafter referred to as the "average strain assumption multiplier", ε_{avg} - θ. Table 3 shows the ε_{avg} - θ multiplier for the Y1@X3~X4 beam at each floor. Note that because the beams are T-shaped, and different values are given depending on whether the beam is in tension at the top or bottom, there are a total of four possible ε_{avg} - θ multipliers.

By multiplying the beam rotation time history by the $\varepsilon_{avg} - \theta$ multiplier, the strain time history of the beam's longitudinal bars can be obtained. Fig. 6 shows the strain history of the longitudinal bars for the floor with the highest beam rotation for each seismic wave. Note that the values in Fig. 6 are for the bottom rebar. Only the maxima or minima of the plastic deformation portions (ε_{avg} > 0.2%) are plotted. Fig. 6 shows that tensile deformation dominates the strain in the longitudinal bars. This is because during compression of the section, the concrete bears most of the compressive stress in the member. The maximum value of the strain ε of the rebar is 1.7%, indicating that strain ε exceeding 1% occurs only during the first few cycles.

Table 3. Average strain assumption $\varepsilon_{avg} - \theta$ of each Floor.

Floor	Lower end tension		Upper end tension	
	Lower end	Upper end	Lower end	Upper end
RF	1.54	0.18	0.41	1.31
9~10F	1.42	0.21	0.45	1.18
7~8F	1.41	0.18	0.41	1.18
5~6F	1.45	0.15	0.37	1.22
2~4F	1.49	0.20	0.44	1.25
1F	1.56	0.11	0.35	1.32

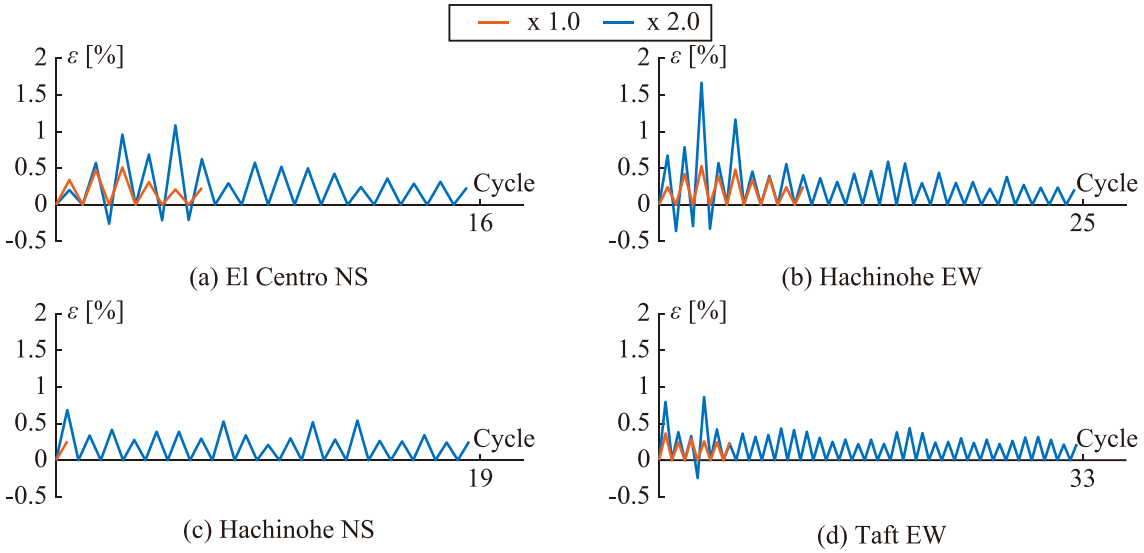

Fig. 6. Main reinforcement strain ε time history of beam when assuming average strain.

3.3 Experimental investigation: beam member loading test overview[9)]

Three RC beam specimens (G2, G4 and G5) were fabricated using identical reinforcement layout as part of a previous study[9)]. The specimen drawings and instrumentation are shown in Fig. 7. As shown in Fig. 7, 18 displacement transducers (E1~E9, W1~W9) were installed along the beam edges to measure the member local vertical deformations. Since the beam width is 280 mm, the hinge length is assumed to be 140 mm, and the beam rotation angle is calculated from the measurement results of four of the

displacement transducers in the hinge (E1, E2, W1, and W2). The strain in the longitudinal bars (Grade SD345, 13 mm diameter) was measured by strain gauges attached at three cross-sections shown as the red circles in Fig. 7. The ε_{YH} for the longitudinal reinforcement is 1.84% based on the material test results.

The loading cycles of the specimen are shown in Fig. 8. The G2 and G4 specimens were subjected to two cycles at each deformation angle, and the G5 specimen was pushed through to failure after 20 cycles of force, as shown in Fig. 8.

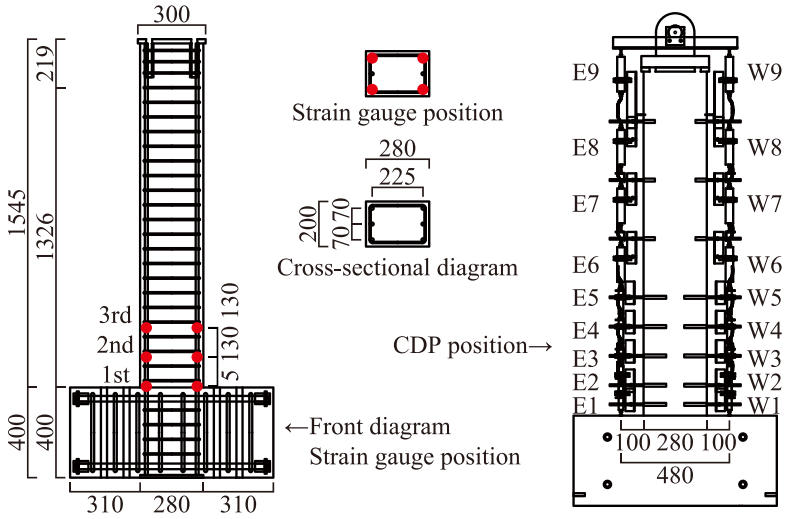

Fig. 7. Beam specimen drawings.

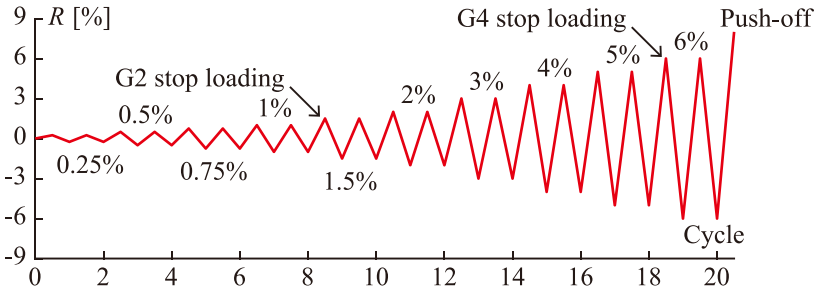

Fig. 8. Beam test loading cycle history.

3.4 Beam member loading test results and comparison to analytical

Fig. 9 shows the maximum value ε_{max} of the measured longitudinal bar strain for the beam rotation angle θ obtained from the experimental results. Note that the rebar yielding in compression is excluded. The black line in Fig. 9 indicates ε_{avg}-θ relationship if calculated based on the average strain assumption and using the specifications of the beam specimen shown in Table 4. Fig. 9 shows that unlike the strain determined from analytical results in the previous sections (1.7% at 0.012 rad rotation), the experimental reinforcement strain is considerably higher at 2.3% (shown as the horizontal dotted line). As shown in Fig. 9, the main bar strain increases rapidly after a certain point and is not linear as assumed using the average strain assumption. Thus, the average strain assumption is not valid for initial loading - this is likely due to the occurrence of high local strains at locations of concrete cracks. Since strain ageing is a local effect, the expected local strains measured at crack locations should be considered explicitly, as opposed to smearing strain over a pre-defined hinge area. Therefore, to better represent the expected reinforcement strains, ε_{exp}, in the 'small rotation' region, a regression line is fitted to the data in Fig. 9, using Eq. (15) below.

$$\varepsilon_{\exp} = \frac{1.9}{1 + e^{(-1400\theta + 4)}} \text{ but no lower than } \varepsilon_{\text{avg}} \text{ (average strain assumption)} \qquad (15)$$

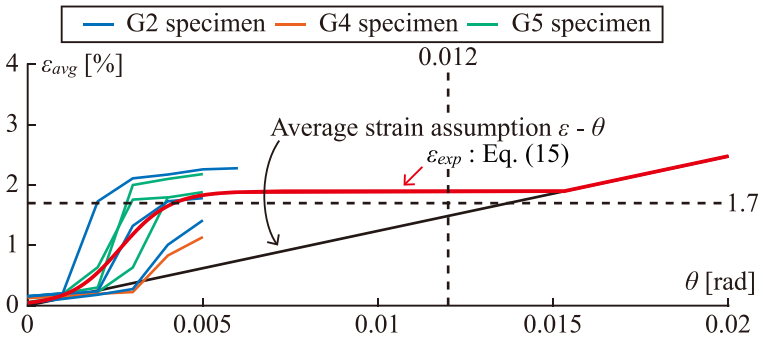

Fig. 9. $\varepsilon_{\max}$ for beam rotation angle θ obtained from results of beam loading test.

Table 4. Specifications and average strain assumption $\varepsilon - \theta$ of beam specimen.

Dimension	Main reinforcement	Stirrups	Side bar	Average strain assumption $\varepsilon - \theta$ Tension	Compression
200×280	6-D13(SD345)	2-D6(SD295)	-	1.24	0.36

4 Response of structure after strain ageing

Using Eq. (15) and Fig. 9, the analytical building model described in section 3.1 is adjusted to account for the reinforcement yield strength increases due to strain ageing. Fig. 10 shows typical beam main reinforcement strain before and after correction. In addition, in Fig. 10, the strain ε_{YH} at the start of strain hardening is shown by a dotted line. From Eq. (6) and (9), it is calculated that the yield strength of reinforcing bars exceeding a strain of ε_{YH} would increase by 15% and that of other reinforcing bars by 4%. Based on these material property changes, the moment-rotation characteristics of the lumped plasticity spring models of the beams in the structure were adjusted. Fig. 10 shows typical beam main reinforcement strain before and after correction. Fig. 11 shows the typical lumped plastic hinge backbone model before and after adjustment. It is noted that ultimate hinge deformation capacity would reduce as a result of strain ageing effects; however, this effect is not accounted for in the present model as the expected deformation demands are far from approaching the ultimate deformation capacity.

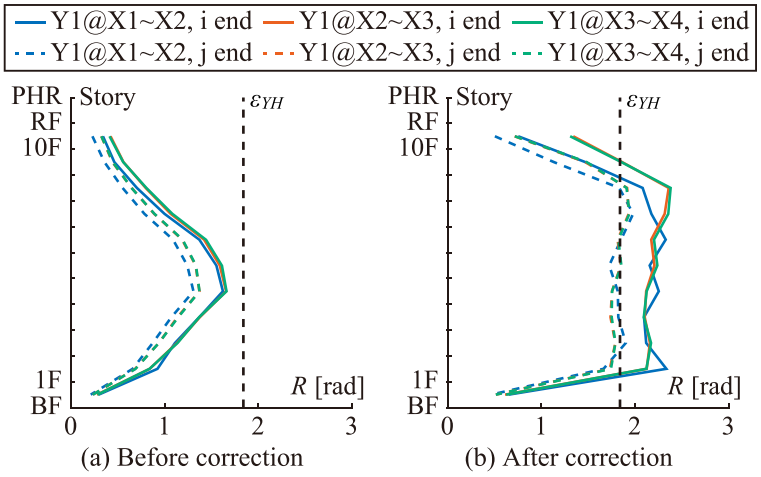

Fig. 10. $\varepsilon_{\max}$ for beam rotation angle θ obtained from results of beam loading test.

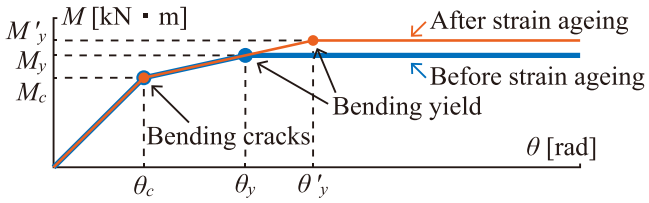

Fig. 11. Schematic diagram of restoration properties of beam.

Fig. 12 shows a comparison of the static pushover analysis results before and after the effects of reinforcement strain ageing, and Fig. 13 shows a comparison of the maximum story drift angle R from the time history analysis using ground motions from Fig. 4. Note that limit state 1 and limit state 2 in Fig. 12 indicate when the retained horizontal strength is reached and when shear failure occurs, respectively. From Fig. 12 and 13, it can be seen that there is little difference in the response results before and after the increase in reinforcement yield strength due to strain ageing. The reason for this is thought to be that the created building model has high stiffness and hinge deformations are only slightly above yielding. Thus, for buildings with minimal yielding after an earthquake, changes in characteristics due to strain ageing have little effect on seismic response in future earthquakes. In the future, buildings with low stiffness (common in countries like NZ and US, that rely heavily on ductility), will also be investigated to analyze the effects of strain ageing on change in global response characteristics as well as local member failure hierarchies.

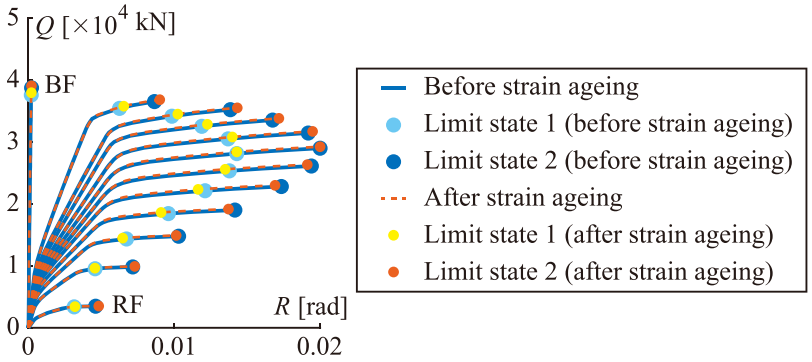

Fig. 12. Comparison of static incremental analysis.

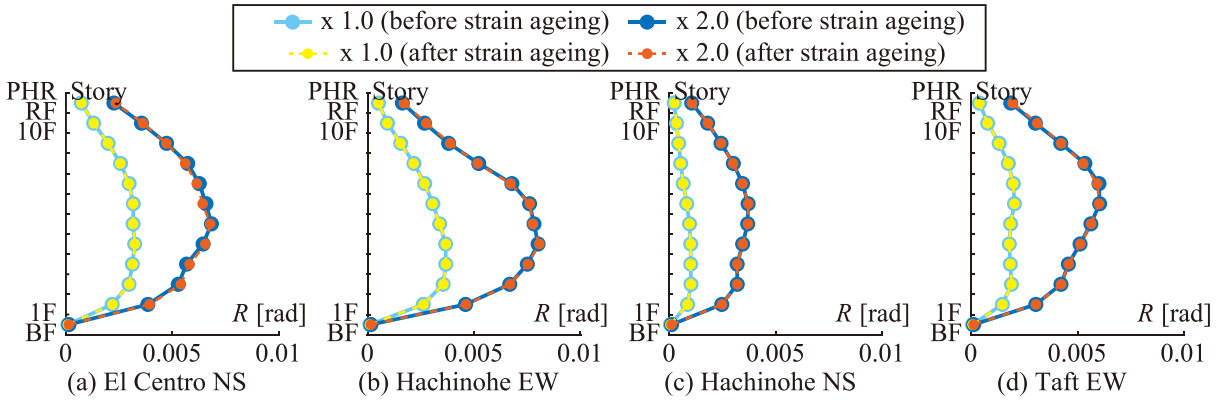

Fig. 13. Comparison of maximum interlayer deformation angle R during seismic response analysis.

5 Summary

In this study, the effects of strain ageing on the future performance of RC buildings damaged by earthquakes are investigated. Firstly, a predictive model is introduced based on previous experimental studies to quantify the change in reinforcement properties as a result of strain ageing. This model is then

utilized to alter the plastic hinge characteristics of an RC building model. The study results are summarized below.

1) From seismic response analysis of a representative Japanese RC building, the maximum beam rotation θ was found to be in the order of 0.012 rad for a Design Level 2 earthquake demand. Using an average strain assumption, the maximum strain of the reinforcing bars under this condition ε was determined to be 1.7%.
2) From RC beam member experiments, the maximum strain on the reinforcing bars ε was found to be in the order of 2.3% at beam hinge rotation angles below 0.012 rad. This indicates that the average strain assumption is not reliable due to the presence of localized concrete cracks.
3) A simple relationship for expected strains in the members of the analytical model was used to determine the degree of strain ageing in the reinforcing steel following an earthquake. The response of the building model adjusted for the effects of strain ageing showed no major differences in future earthquake response. The reason for this is thought to be the inherently high stiffness of Japanese RC buildings resulting in limited yielding. Further studies are to be conducted on more flexible buildings typical in other countries.

Acknowledgements

This work was supported by JSPS KAKENHI Grant Number 22K14315. The authors also acknowledge the kind support provided by Tokyo Tekko company for providing the reinforcing material used to conduct this study. Finally, acknowledgements are given to students of Sato-lab at Tokyo Institute of Technology who assisted in performing the experimental work.

References

1. A.V. Shegay, K. Okamura, D. Sato: Predictive models for changes in reinforcement characteristics due to strain ageing effects, New Zealand Society for EarthQuake Engineering, 2023.
2. Hundy B.B.: Accelerated strain ageing of mild steel, Journal of the Iron and Steel Institute, pp. 34-38, 1954.
3. Loporcaro G., Pampanin S., Kral M.V.: Long-term strain-ageing effects on low carbon steel reinforcement, Construction and Building Materials, 2019.
4. Momtahan A., Dhakal R.P., Rieder A.: Effects of strain-ageing on New Zealand reinforcing steel bars, Bulletin of the New Zealand Society for Earthquake Engineering, 42(3), pp.179-186, 2009.
5. Pussegoda L.N.: Strain age embrittlement in reinforcing steels, University of Canterbury, Ph. D thesis, 1978.
6. Structural Design and component cross section examples, Japan Building Disaster Prevention Association, 2007.
7. RESP-D user manual, Kozo Keikaku Engineering Inc., 2019.
8. Reinforced concrete construction calculation standards and commentary, Architectural Institute of Japan, 2007.
9. M. Masaki, et al: Study on the structural performance and damage characteristics of repaired flexural RC members by static loading test Part1-Part5, Summaries of technical papers of annual meeting, Architectural Institute of Japan, pp.425-434, 2022.